

Revealing single emitter spectral dynamics from intensity correlations in an ensemble fluorescence spectrum

Xavier Brokmann¹, Lisa Marshall², Mounji Bawendi²

¹20 rue Barbanègre, F-75019 Paris.

²Massachusetts Institute of Technology 77 Massachusetts Avenue, Cambridge MA 02139.

xbrokmann@gmail.com

Abstract: We show that the single emitter linewidth underlying a broadened ensemble emission spectrum can be extracted from correlations among the stochastic intensity fluctuations in the ensemble spectrum. Spectral correlations can be observed at high temporal and spectral resolutions with a cross-correlated pair of avalanche photodiodes placed at the outputs of a scanning Michelson interferometer. As illustrated with simulations in conjunction with Fluorescence Correlation Spectroscopy, our approach overcomes ensemble and temporal inhomogeneous broadening to provide single emitter linewidths, even for emitters under weak, continuous, broadband excitation.

OCIS codes: (030.5290) Photon statistics ; (300.6280) Spectroscopy, fluorescence and luminescence.

References and links

1. L. Mandel and E. Wolf, *Optical Coherence and Quantum Optics* (Cambridge University Press, 1995).
 2. V.S. Zapasskii and G.G. Kozlov, "Correlation analysis of spectral fluctuations in inhomogeneously broadened spectra," *Opt. Express* **8**, 509–516, 2001.
 3. F. Intonti, V. Emiliani, C. Lienau, Th. Elsaesser, V. Savona, E. Runge, R. Zimmermann, R. Notzel, and K.H. Ploog, "Quantum mechanical repulsion of exciton levels in a disordered quantum well," *Phys. Rev. Lett.* **27**, 0768011–4 2001.
 4. G. von Freymann, U. Neuberth, M. Deubel, M. Wegener, G. Khitrova, and H.M. Gibbs, "Level repulsion in nanophotoluminescence spectra from single GaAs quantum wells," *Phys. Rev. B* **65**, 2053271–9, 2002.
 5. X. Brokmann, M.G. Bawendi, L. Coolen, and J.P. Hermier, "Photon-correlation Fourier spectroscopy," *Opt. Express* **14**, 6333–6341, 2006.
 6. D. Magde, E.L. Elson, and W.W. Webb, "Fluorescence Correlation Spectroscopy 2. Experimental Realization" *Biopolymers* **33**, 29–61, 1974.
-

1. Introduction

Single emitters often display dynamic and complex behaviors entirely masked by ensemble measurements. Spectroscopy on these emitters has reached impressive heights. There are systems, however, where it is not feasible or desirable to separate the individual emitter from the ensemble. When confronted with the task of isolating individual properties from large populations, spectroscopy offers a variety of dedicated responses such as Doppler-free, hole-burning and photon-echo spectroscopies [1] to resolve ensemble and temporal averaging effects encountered in inhomogeneously and homogeneously broadened samples. These diverse and powerful techniques share a common trait; they all rely on the nonlinear optical properties of the emitters.

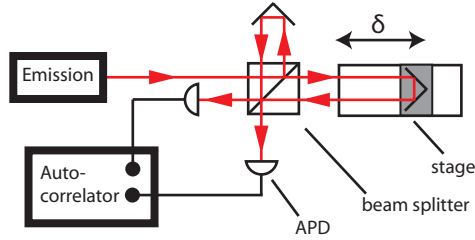


Fig. 1. Our approach uses an interferometer to convert fast spectral fluctuations into intensity fluctuations. The cross-correlation of the fluctuations in the interferometer outputs reveals single emitter spectral dynamics with high temporal and spectral resolution.

Hence, they tend to perform poorly on emitters with a small or vanishing optical nonlinearity and questionably on samples too delicate to handle the high excitation power required for non-linear optics.

Surprisingly, methods to extract the linewidth of a single emitter from a broadened ensemble spectrum under the more gentle conditions of linear excitation remain more elusive. In principle, the single emitter linewidth can be determined from correlations among the stochastic fluctuations in the ensemble emission spectrum [2]. Progress in this direction was demonstrated in previous works investigating the autocorrelation of the broad spectrum of disordered nanostructures [3, 4]. Due to the long duration necessary to record a high resolution spectrum, that approach cannot resolve the fast temporal broadening effects found in most inhomogeneous samples, severely limiting the ability to measure an underlying single emitter linewidth.

In this Letter, we describe an experimental method revealing spectral correlations of a single emitter with high spectral and temporal resolution, despite the single emitter spectrum being obscured by an ensemble emission spectrum. The approach - shown in Figure 1 and reminiscent of our previous work on Photon Correlation Fourier Spectroscopy [5] - consists of using a scanning Michelson interferometer to turn spectral correlations in the broadened spectrum into intensity correlations recorded by a Hanbury Brown Twiss detection setup. Previously, we applied this method to an isolated single emitter. Here, we expand and generalize to obtain the same dynamic single emitter spectral information from an ensemble of emitters. The method is investigated theoretically and demonstrated with numerical simulations illustrating its significance in conjunction with Fluorescence Correlation Spectroscopy (FCS).

2. Intensity correlations in an inhomogeneous spectrum

We introduce here the various quantities necessary to describe intensity correlations in an inhomogeneous spectrum and then describe a potential experimental setup dedicated to their measurement.

2.1. Theoretical description

We consider a collection of N nearly identical emitters embedded in a dynamic and spatially inhomogeneous environment. Due to slight variations in the structure of the emitters (e.g. in their shape or composition) and spatial inhomogeneity (as caused, for example, by nanoscale disorder for emitters in a condensed medium), the spectra of the single emitters do not collapse on a single narrow, homogeneous stationary spectral line, but instead disperse their averaged frequencies $\omega_1, \dots, \omega_i, \dots, \omega_N$ over a spectral width Δ around some frequency ω_0 (Figure 2a). Temporal inhomogeneities additionally cause the lineshapes of the emitters, $s_1(\omega, t), \dots, s_i(\omega, t), \dots, s_N(\omega, t)$, to be explicitly dependent on time t , each emission line un-

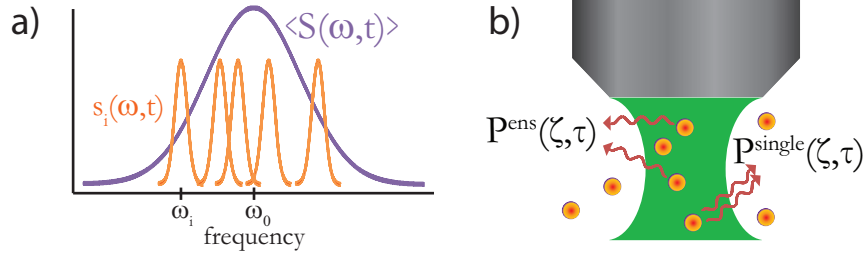


Fig. 2. Single-emitter and ensemble spectral correlations in the fluorescence of a population of emitters. a) We first consider an ensemble of emitters with the same narrow line shape but different center frequencies. The ensemble spectrum would appear as a broad Gaussian $\langle S(\omega, t) \rangle$. b) With our setup, intensity correlations from the emission of single emitters flowing under a microscope objective will contribute to the single emitter spectral correlation, $P^{\text{single}}(\zeta, \tau)$, if the two photons correlated are from the same emitter. Correlations of photons originating from different emitters will provide the ensemble spectral correlation, $P^{\text{ens}}(\zeta)$.

dergoing independent, identically distributed temporal stochastic spectral fluctuations over a mean-squared range $\sigma^2 = \langle [s_i(\omega, t) - \omega_i]^2 \rangle$ centered around the single emitter's average transition frequency ω_i (where $\langle \cdot \rangle$ denotes the average over many independent observations). At any time t , each emitter contributes to the ensemble emission with an intensity $I_i(t) = \int s_i(\omega, t) d\omega$ and a normalized lineshape $\hat{s}_i(\omega, t) = s_i(\omega, t)/I_i(t)$ (i.e. $\int \hat{s}_i(\omega, t) d\omega = 1$).

Stochastic fluctuations in the total intensity of the spectrum $I(t) = \sum_{i=0}^N I_i(t)$ are traditionally approached through the second-order (intensity) correlation function $g^{(2)}(\tau) = \langle I(t)I(t + \tau) \rangle / \langle I(t) \rangle^2$. Similarly, fluctuations in the ensemble spectrum $S(\omega, t) = \sum_{i=0}^N s_i(\omega, t)$ can be analyzed through the spectral correlation function $P(\zeta, \tau)$:

$$P(\zeta, \tau) = \left\langle \int S(\omega, t) S(\omega + \zeta, t + \tau) d\omega \right\rangle. \quad (1)$$

Qualitatively, the spectral correlation function $P(\zeta, \tau)$ scales as the probability to measure a frequency difference ζ between two photons separated by a time interval τ . Important properties of $P(\zeta, \tau)$ appear when splitting up Eq.1 into two distinct components as :

$$P(\zeta, \tau) = P^{\text{ens}}(\zeta, \tau) + P^{\text{single}}(\zeta, \tau) \quad (2)$$

where $P^{\text{ens}}(\zeta, \tau) = \sum_{i \neq j} \int \langle s_i(\omega, t) s_j(\omega + \zeta, t + \tau) \rangle d\omega$ and $P^{\text{single}}(\zeta, \tau) = N \langle \int s_i(\omega, t) s_i(\omega + \zeta, t + \tau) d\omega \rangle$. Since emitters have statistically independent fluctuations, the component $P^{\text{ens}}(\zeta, \tau)$ rewrites as $P^{\text{ens}}(\zeta, \tau) = \sum_{i \neq j} \int \langle s_i(\omega, t) \rangle \langle s_j(\omega + \zeta, t) \rangle d\omega$, i.e. $P^{\text{ens}}(\zeta, \tau)$ is independent of τ and reduces to the autocorrelation of the average ensemble spectrum. Similarly, $P^{\text{single}}(\zeta, \tau)$ reduces to the autocorrelation of the time-averaged single emitter spectrum as long as the single emitter spectra $s_i(\omega, t)$ and $s_i(\omega, t + \tau)$ are uncorrelated, i.e. for large values of τ . But on shorter timescales $\tau \rightarrow 0$, temporal inhomogeneous broadening is suppressed as no spectral fluctuations have time to occur, and $P^{\text{single}}(\zeta, \tau = 0)$ coincides with the autocorrelation of the single emitter spectrum. The difference between $P^{\text{single}}(\zeta, \tau = 0)$ and $P^{\text{ens}}(\zeta)$ is illustrated in Figure 2b.

Information on the linewidth of the single emitter hence appears systematically encoded into the spectral correlation function $P(\zeta, \tau)$. As shown below, the spectral correlation function $P(\zeta, \tau)$ turns out to be a quantity that can be measured directly with a dedicated experiment from which the single emitter linewidth can be extracted.

2.2. Measurement setup

The experiment involves a setup previously introduced to observe the spectral dynamics of an isolated emitter at high temporal resolution [5]. The emission is sent to a Michelson interferometer with an arm continuously moving back and forth (at velocity V) over a range of several fringes around an optical path difference δ . The intensities $I_a(t), I_b(t)$ at the outputs of the interferometer oscillate as the Fourier transform of the emission spectrum

$$I_{a,b}(t) = \sum_{i=1}^N I_i(t) \left[1 \pm \int_0^\infty \hat{s}_i(\omega, t) \cos(\omega \delta(t)/c) d\omega \right], \quad (3)$$

where $\delta(t)$ is the instantaneous optical path difference between the arms ($\overline{\delta(t)} = \delta$). A pair of avalanche photodiodes detects these intensities and a photon-counting board computes their cross-correlation function $g^\times(\tau)$:

$$g^\times(\tau) = \frac{\overline{I_a(t) I_b(t + \tau)}}{\overline{I_a(t)} \overline{I_b(t + \tau)}}, \quad (4)$$

where $\overline{\dots}$ indicates time-averaging over acquisition time of the intensity correlation.

Assuming the scanning speed V is set low enough to ensure that fringes oscillate on the photodiodes with a temporal periodicity $c/2\omega_0 V$ larger than the timescales τ under investigations, the time-averaged intensity cross-correlation function $g^\times(\tau)$ measured at the output of the scanning interferometer decomposes as

$$g^\times(\tau) = g^{\text{ens}}(\tau) + g^{\text{single}}(\tau), \quad (5)$$

with :

$$g^{\text{ens}}(\tau) = \frac{N-1}{N} \left(1 - \frac{1}{2} \text{FT}[p^{\text{ens}}(\zeta)]_{\delta/c} \right) \quad (6)$$

$$g^{\text{single}}(\tau) = \left(g^{(2)}(\tau) - 1 + \frac{1}{N} \right) \times \left(1 - \frac{1}{2} \text{FT}[p^{\text{single}}(\zeta, \tau)]_{\delta/c} \right) \quad (7)$$

where $p^{\text{ens}}(\zeta) = P^{\text{ens}}(\zeta) / \int P^{\text{ens}}(\zeta) d\zeta$ and $p^{\text{single}}(\zeta, \tau) = P^{\text{single}}(\zeta, \tau) / \int P^{\text{single}}(\zeta, \tau) d\zeta$ denote the normalized spectral correlation functions of the ensemble spectrum and single-emitter spectrum respectively.

This result simplifies in a few important cases. For an isolated emitter ($N = 1$), the cross-correlation function $g^\times(\tau)$ reduces to its single-emitter component, i.e. $g^\times(\tau) = g^{\text{single}}(\tau)$. Assuming the emission obeys Poissonian statistics (i.e. $g^{(2)}(\tau) = 1$), the intensity cross-correlation function reads :

$$g^\times(\tau) = 1 - \frac{1}{2} \text{FT} \left[p^{\text{single}}(\zeta, \tau) \right]_{\delta/c}, \quad (8)$$

in agreement with previous theoretical findings [5]. In this case, the cross-correlation function $g^\times(\tau)$ depends on the value in δ/c of the Fourier transform (in ζ) of the single emitter spectral correlation function $p^{\text{single}}(\zeta, \tau)$. Hence, the dynamics of the single emitter linewidth (as encoded in $p^{\text{single}}(\zeta, \tau)$) can be reconstructed through the successive accumulation of cross-correlation functions $g(\tau)$ at various optical path differences δ .

Our main point is that the single-emitter component $g^{\text{single}}(\tau)$ in the cross-correlation function $g^\times(\tau)$ does not vanish even when the number of emitters involved in the experiment becomes very large ($N \gg 1$), provided photoemission occurs with non-Poissonian statistics (i.e. $g^{(2)}(\tau) \neq 1$). Indeed, Equations 5-7 then rewrite as

$$g^\times(\tau) = g^{(2)}(\tau) - \frac{1}{2} \text{FT} \left[p^{\text{ens}}(\zeta) + (g^{(2)}(\tau) - 1) p^{\text{single}}(\zeta, \tau) \right]_{\delta/c}, \quad (9)$$

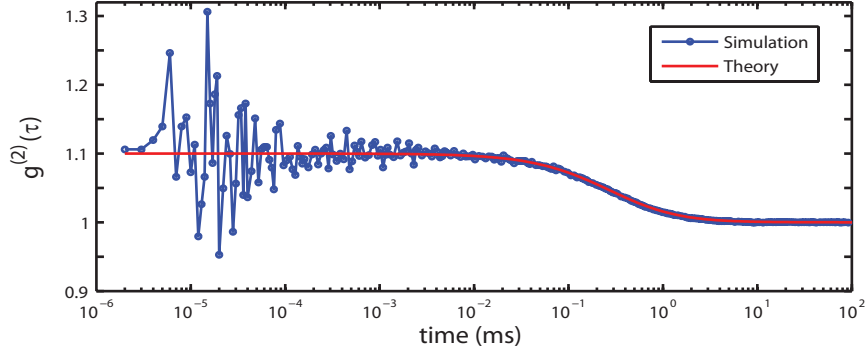


Fig. 3. The standard FCS intensity correlation function, $g^{(2)}(\tau)$. Our method works in situations like FCS, where the ensemble emission exhibits an intensity correlation function $g^{(2)}(\tau) \neq 1$ at short timescales. In these cases, the single emitter spectral correlation, $p^{\text{single}}(\zeta, \tau)$, is weighted by $g^{(2)}(\tau) - 1$ and can be separated from the background ensemble spectral correlation, $p^{\text{ens}}(\zeta)$.

where the normalized cross-correlation function $g^{\times}(\tau)$ contains contributions from both the inhomogeneous ensemble and single-emitter spectra, with magnitudes of order 1 and $g^{(2)}(\tau) - 1$ respectively (Figure 3). Information on the single emitter spectrum will therefore survive ensemble averaging when emitters, for example, radiate intermittently, as seen on blinking or transiently-excited emitters - for which $g^{(2)}(\tau \rightarrow 0) = 1 + 1/n$, where n is the time-averaged number of emitters significantly contributing to the ensemble spectrum at any time. The result also holds for emitters showing complete photon antibunching (i.e. individually behaving as single-photon sources), for which $g^{(2)}(\tau \rightarrow 0) = 1 - 1/n$.

We also note that recording cross-correlation functions $g^{\times}(\tau)$ over long durations raises the signal-to-noise ratio, thus improving the measurement of the homogeneous linewidth - a result in complete contrast with standard spectroscopy, where longer accumulation times yield higher signal-to-noise ratios at the expense of greater inhomogeneous broadening.

3. Application: unveiling spectral fluctuations in Fluorescence Correlation Spectroscopy

Fluorescence Correlation Spectroscopy (FCS) [6] provides a well-defined framework to illustrate these findings and their significance. We choose two examples to simulate. In our first example, we model an ensemble comprised of single emitters with differing center frequencies, ω_i , and fixed doublet spectrum consisting of two delta functions at $\omega_i - \frac{\Omega}{2}$ and $\omega_i + \frac{\Omega}{2}$. As shown below, the underlying doublet is easily resolved from the broad ensemble spectrum with our method, despite the lack of evidence for a doublet in the ensemble emission spectrum (Figure 4). In our second example, we allow the center frequency of each doublet to fluctuate in time with a frequency $\omega_i(t)$ and demonstrate our ability to observe these spectral dynamics (Figure 5).

3.1. Numerical methods

We modeled FCS experiments by simulating photodetection times and emission wavelengths for spherical emitters of 2 nm radius freely diffusing in water at room temperature (diffusion coefficient $D = 100 \mu\text{m}^2/\text{s}$) and excited by a tightly focused beam forming a spherical Gaussian excitation spot of width $w_0 = 200$ nm. The concentration of the emitters in the solution was adjusted so that a number of emitters $n = 10$ were found in the excitation volume at any time.

Detection of the fluorescence from the excitation spot was set to a total photodetection rate of $I = 10^5$ counts/s.

FCS simulations were performed by generating three-dimensional Brownian motion trajectories for N emitters diffusing in a finite, cubic-shaped, open volume simulation box centered on the excitation spot. To do so, the diffusion trajectories of N particles were first computed in unbounded free-space, and then subsequently put into the bounded simulation box by considering the latter as the unit cell of a three-dimensional tiling with periodic boundary conditions. A concentration of $n = 10$ emitters under the laser spot was reached for a total number of emitters $N = 10^5$ in the simulation box. Once the single-emitter trajectories were computed, each of the N emitters was assigned a center frequency ω_i drawn from the underlying Gaussian ensemble distribution of width Δ centered on ω_0 . Open volume conditions were enforced by redrawing the wavelength of an emitter from this distribution every time it reached a boundary of the simulation box.

Computations of Brownian trajectories can be highly demanding when high temporal and spatial resolution are required, as is the case in FCS. However, the problem simplifies by noting that the position of an emitter needs only to be determined when it creates a photodetection event. The positions of each emitter were therefore first computed assuming uniform excitation over the simulation box, i.e. at times separated by intervals distributed with Poissonian statistics. Non-uniform excitation over the simulation box was then taken into account by filtering these photodetection times with a survival probability $p = \exp(-\mathbf{r}^2/2w_0^2)$ given by the Gaussian excitation profile at the emitter's location \mathbf{r} . Emitters far from the excitation spot at a given time do not radiate, and so do not contribute to the FCS signal, making the computation of their trajectory at that time unnecessary. The width of the simulation box ($4 \mu\text{m}$) was therefore kept minimal, yet large enough compared to the excitation spot size $w_0 = 200 \text{ nm}$ to keep finite simulation box effects negligible.

Implemented in C (Anjuta 2.4.1) on a personal computer (1 GHz CPU, Linux), the above procedure typically required a few hours to produce long streams of photodetection events consisting of more than 10^7 photodetection times with their associated detected wavelength for emitters freely diffusing in a liquid environment under focused laser excitation. The validity of our approach was confirmed by excellent agreement between the simulated and theoretical intensity correlation functions $g^{(2)}(\tau)$ expected from FCS experiments on spherical shaped emitters in water (Figure 3).

3.2. Line shape of single emitters with static spectra revealed despite ensemble broadening

In our first example, ensemble emission was centered at a wavelength $\lambda_0 = 600 \text{ nm}$, with individual transition frequencies $\omega_1, \dots, \omega_i, \dots$ distributed around λ_0 with Gaussian statistics over a FWHM range $\Delta = 6 \text{ nm}$ as expected from slight but significant inhomogeneous broadening. Each single emitter spectrum consisted of a doublet of monochromatic lines separated by a spectral width $\Omega = 1 \text{ nm}$.

If measured with a conventional FCS detection setup, the correlation function $g^{(2)}(\tau)$ of the sample peaks at short timescales $\tau \ll \tau_D$ (Figure 3), accounting for the fact that the total detected intensity $I(t)$ fluctuates as emitters continuously enter and exit the excitation volume with an average diffusion time $\tau_D = w_0^2/4D = 100 \mu\text{s}$. Here, an emitter therefore diffuses out of the spot within a duration τ_D comparable to the average delay $n/I = 100 \mu\text{s}$ between its detected photons, hence contributing to the total fluorescence signal by a few photons at most. Under such conditions, the spectrum observed in standard spectroscopy reduces to its inhomogeneous component - namely a broad Gaussian line of width $\Delta \gg \Omega$. The doublet in the single emitter spectrum is not detected (Figure 4a).

We then add the Michelson interferometer in the photodetection path and scan the interfer-

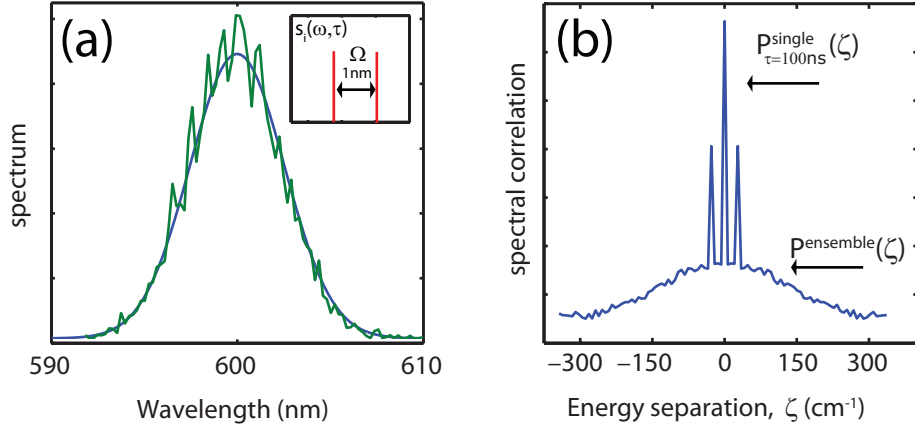


Fig. 4. Standard spectroscopy versus spectral correlation measurement. a) Emission spectrum as measured by standard spectroscopy after an acquisition time of 1 s. The corresponding lineshape coincides with the average ensemble spectrum, $\langle S(\omega, t) \rangle$, and shows no evidence of the underlying single-emitter doublets $s_i(\omega, t)$. b) Using our method, the spectral correlation of the underlying doublet, $p^{\text{single}}(\zeta, \tau)$, is easily seen on top of a broad ensemble pedestal, $p^{\text{ens}}(\zeta)$. The amplitude of $p^{\text{single}}(\zeta, \tau)$ is determined by the intensity correlation function $g^{(2)}(\tau)$ of the sample emission.

ometer continuously over 10 fringes around various optical path differences δ . The scanning speed V is set to 5 fringes/s to access the spectral dynamics at all timescales $\tau < c/2\omega_0 V = 200$ ms. Each cross-correlation function $g^\times(\tau)$ is measured by accumulating photons over 1 minute.

The cross-correlation function $g^\times(\tau)$ now shows a strong dependence on the optical path difference δ where it was recorded, which directly provides the normalized spectral correlation function $p(\zeta, \tau) = p^{\text{ens}}(\zeta) + (g^{(2)}(\tau) - 1)p^{\text{single}}(\zeta, \tau)$ by taking the inverse Fourier transform in Eq.9. Photons separated by durations $\tau \gg \tau_D$ can not be spectrally correlated, since the population of emitters in the focal spot undergoes complete renewal over timescales $\tau \sim \tau_D$, accounting for the fact that $p(\zeta, \tau)$ then coincides with $p^{\text{ens}}(\zeta)$. On timescales shorter than τ_D , emitters generally do not have time to diffuse out of the excitation spot. Photons separated by durations $\tau < \tau_D$ have a non-zero probability $g^{(2)}(\tau) - 1$ of being from the same emitter and therefore containing information from a single emitter. It is at these timescales that the underlying doublet is revealed, as seen from the triplet of lines of relative amplitude $\{1/4, 1/2, 1/4\}$ at frequencies $\{-\Omega, 0, +\Omega\}$ produced by the autocorrelation of a doublet of width Ω (Figure 4b).

3.3. Line shape of single emitters with a dynamic spectrum

The method also yields results on single emitters with a dynamic spectrum. Simulations were performed for emitters with a doublet spectrum of width $\Omega = 1$ nm undergoing both static broadening over a FWHM range $\Delta = 6$ nm and individual dynamic Gaussian spectral fluctuations with a correlation time $\tau_c = 100 \mu\text{s}$ over a broad FWHM spectral range $\sigma = 3$ nm around their center frequencies ω_i . All other parameters (emitter radius, scanning speed, detection intensity etc.) were left unchanged from previous section.

In this case, the time-averaged spectrum is a broad Gaussian, while the time-resolved spectrum is a doublet of separation $\Omega = 1$ nm. Here again, standard spectroscopy cannot provide the single emitter linewidth, as spectral broadening caused by diffusion under the excitation spot and spectral diffusion of the single emitter happens at a rate $\tau_D^{-1} + \tau_c^{-1} = 20 \text{ ms}^{-1}$ faster than

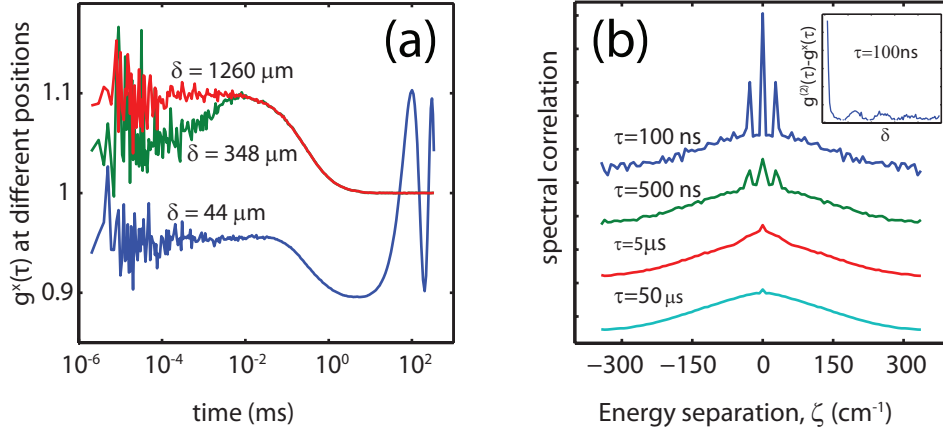


Fig. 5. Intensity cross-correlations at the outputs of the scanning interferometer for a population of emitters undergoing both static and dynamic spectral broadening. a) $g^\times(\tau)$ as measured at different interferometer positions δ . The cross-correlation functions $g^\times(\tau)$ differ from the standard FCS intensity correlation function $g^{(2)}(\tau)$ at long timescales $\tau \gg \tau_D$ due to the ensemble spectral correlation $p^{\text{ens}}(\zeta)$ and at short timescales $\tau \ll \tau_D$ due to the time-dependent single-emitter spectral correlation function $p^{\text{single}}(\zeta, \tau)$. b) Decay of the $g^\times(\tau)$ with δ at short timescale $\tau = 100$ ns (insert). The corresponding Fourier transform of $g^{(2)}(\tau) - g^\times(\tau)$ for increasing values of τ reveals the time dependent single emitter spectral correlation, $p^{\text{single}}(\zeta, \tau)$.

the average single-emitter photodetection rate $I/n = 10 \text{ ms}^{-1}$.

Figure 5a shows $g^\times(\tau)$ for several different interferometer positions δ . The corresponding patterns in the correlation functions $g^\times(\tau)$ can be understood as follow. For optical path differences δ comparable to the ensemble coherence length $\Lambda = \Delta/c = 40 \text{ } \mu\text{m}$, the output intensities are strongly modulated by the interference pattern of the ensemble spectrum, correspondingly producing strong intensity anticorrelations between the interferometer outputs at every timescale τ ($\delta = 44 \text{ } \mu\text{m}$, Figure 5a). If we now increase the optical path difference δ until the ensemble coherence length Λ is exceeded, fringes emanating from the ensemble spectrum completely vanish ($\delta = 348 \text{ } \mu\text{m}$, Figure 5a). In this regime, distortions from the correlation function seen in standard FCS (and in Figure 3) nonetheless persist due to single-emitter interference phenomena. Indeed, when plotting $g^\times(\tau)$ as a function of δ , a beatnote is then evidenced at very short timescales $\tau < 100$ ns, showing that the doublet is resolved over delays $\tau \ll \min(\tau_c, \tau_D)$, in agreement with our previous theoretical analysis (Figure 5b, insert). Finally, for very large optical path differences, all interference phenomena vanish, and the standard FCS correlation function is actually recovered ($\delta = 1260 \text{ } \mu\text{m}$, Figure 5a).

Calculating the inverse Fourier transform of $g^{(2)}(\tau) - g^\times(\tau)$ for different values of τ clearly shows the autocorrelation of a temporally evolving doublet - namely a triplet of intensities $\{1/4, 1/2, 1/4\}$ in $\{-\Omega, 0, +\Omega\}$ superimposed on the broad autocorrelation of the ensemble spectrum (Figure 5b).

4. Conclusion

Our approach overcomes both ensemble and temporal averaging effects in large populations of single emitters to provide the linewidth of a single emitter, even if many emitters are detected simultaneously, with each of them contributing only a few photons to the ensemble spectrum.

We demonstrated our approach with simulations in conjunction with FCS, showing the ability to extract a single emitter line shape from an inhomogeneously broadened ensemble. We then made that line shape time dependent and were able to observe the spectral dynamics with high temporal and spectral resolution.

No assumption was made as to the nature of the excitation beam. Illustrated here under continuous excitation, our approach applies to emitters excited by a broadband lamp or a monochromatic laser. Pulsed excitation is also possible, particularly for the exploration of spectral correlations (e.g. multi-excitonic spectral lines) occurring on timescales shorter than the excited state lifetime of the emitters.

5. Acknowledgments

This work was supported by the Department of Energy grant number DE-FG02-07ER46454.